Accurate Direction–of–Arrival Estimation Method Based on Space–Time Modulated Metasurface

Xinyu Fang, Mengmeng Li, *Senior Member, IEEE*, Juzheng Han, Davide Ramaccia, *Senior Member, IEEE*, Alessandro Toscano, *Senior Member, IEEE*, Filiberto Bilotti, *Fellow, IEEE*, and Dazhi Ding, *Senior Member, IEEE*

***Abstract*— A metasurface (MTS)-based direction of arrival (DoA) estimation method is presented. The method exploits the properties of space–time modulated reflective metasurfaces to estimate in real-time the impinging angle of an illuminating monochromatic plane wave. The approach makes use of the amplitude unbalance of the received fields at broadside at the frequencies of the two first-order harmonics generated by the interaction between the incident plane wave and the modulated metasurface. Here, we first describe analytically how to generate the desired higher order harmonics in the reflected spectrum and how to realize the breaking of the spatial symmetry of each order harmonic scattering pattern. Then, the 1-D omnidirectional incident angle can be analytically computed using +1st- and −1st-order harmonics. The approach is also extended to 2-D DoA estimation by using two orthogonally arranged 1-D DoA modulation arrays. The accuracy of 1-D DoA estimation is verified through full-wave numerical simulations. Compared to conventional DoA estimation methods, the proposed approach simplifies the computation and hardware complexity, ensuring at the same time estimation accuracy. The proposed method may have potential applications in wireless communications, target recognition, and identification.**

***Index Terms*— Direction of arrival (DoA) estimation, metasurface (MTS), space–time modulation.**

I. Introduction

DIRECTION of arrival (DoA) estimation is a key functionality in radar tracking and radio navigation [1], [2], satellite communications on-the-move (SOTM) [3], and smart antenna [4]–[6] systems. It is fundamental for establishing and maintaining communication between two terminals while one is moving with respect to the other. Moreover, it is also needed for the next generations of mobile communication, such as 5G and beyond 5G (B5G), and the future sixth-generation (6G) communication, thus enabling location services for the mobile Internet [7], [8]. In this framework, array signal processing methods are the most common techniques to estimate DoA. Among them, it is worth mentioning techniques based on minimum variance distortion-less response (MVDR) [9], estimation of signal parameters via a rotational invariant (ESPRIT) [10], [11], multiple signal classification (MUSIC) [12], [13], and Bayesian compressive sensing (BCS) [14]. The high performances reached by these techniques are, however, counterbalanced by the need of massive arrays and the use of multiple sensors or channels, intense calculation, and expensive hardware. In this framework, a low in transmission and reflection, such as amplitude [15], polarization [16], propagation direction [17], [18], and, more recently, the frequency content [19]–[22], cost technology, and low-complexity DoA estimation system would represent an important advance in those applications where the angular localization of the transmitter, interfering signals, and users is mandatory.

In the last decades, metasurfaces (MTSs) have demonstrated to be a breakthrough technology in a number of applications, spanning from microwave to optical frequency ranges [23]–[25]. They typically consist of a bidimensional (2-D) periodic array of subwavelength meta-atoms able to control the properties of the incident electromagnetic field. In particular, the control of the spatial and/or temporal characteristics of the interacting fields was made possible thanks to the development of dynamically reconfigurable metasurfaces, using different reconfiguring technologies based on p-i-n diodes [26], [27], varactors [29]–[31], MEMS [32], graphene [33], and liquid crystal [34]. The control can be performed through analogical control signals [20]–[22] or via digital control [35]–[37]. In both cases, the resulting metasurfaces belong to the wider family of space–time metamaterials [38]–[45], which exhibit unprecedented capabilities and find applications in different operative scenarios, such as nonreciprocal structures [19], [46]–[49], arbitrary amplitude and phase programmable systems [50], wireless communications [52]–[54], and spread-spectrum radar camouflaging [55].

In this article, we present and discuss a metasurface-based DoA method that exploits the properties of space–time modulated reflective metasurfaces to estimate in real time the impinging angle of an illuminating monochromatic

Manuscript received 28 December 2021; revised 10 May 2022; accepted 7 June 2022. Date of publication 24 June 2022; date of current version 17 November 2022. This work was supported in part by the Natural Science Foundation of China under Grant 61890541, Grant 62025109, and Grant 61871222; and in part by the Fundamental Research Funds for the Central Universities under Grant 30921011101. The work of Filiberto Bilotti was supported by the Research Contract MANTLES funded by the Italian Ministry of University and Research, under Grant PRIN 2017 n. 2017BHFZKH. *(Corresponding author: Mengmeng Li.)*

Xinyu Fang, Mengmeng Li, Juzheng Han, and Dazhi Ding are with the Department of Communication Engineering, Nanjing University of Science and Technology, Nanjing 210094, China (e-mail: limengmeng@njust.edu.cn; dzding@njust.edu.cn).

Davide Ramaccia, Alessandro Toscano, and Filiberto Bilotti are with the Department of Industrial, Electronic and Mechanical Engineering, Roma Tre University, 00146 Rome, Italy (e-mail: davide.ramaccia@uniroma3.it; alessandro.toscano@uniroma3.it; filiberto.bilotti@uniroma3.it).

Color versions of one or more figures in this article are available at https://doi.org/10.1109/TAP.2022.3184556.

Digital Object Identifier 10.1109/TAP.2022.3184556

plane wave at frequency ω_0. The system is composed of a space–time modulated metasurface and a detecting antenna placed in the far-field region just above it. Here, the DoA estimation is performed by measuring the amplitude unbalance of the reflected fields at the frequencies of the two first-order harmonics, i.e., $\omega_0 \pm \omega_p$, generated by the interaction between the incident plane wave and the metasurface modulated at frequency $f_p = \omega_p/2\pi$. However, we are unable to achieve the DoA estimation by just using the two first-order harmonics without any spatial difference. Due to the typical frequency used for the modulation, i.e., $\omega_p \ll \omega_0$, in fact, the two harmonics exhibit almost identical amplitude, being governed by the Manley–Rowe relations [56], [57]. Here, we exploit the spatial modulation as an additional degree-of-freedom for enhancing the required unbalancing, inducing a pattern asymmetry for the fields scattered at the two first-order harmonics.

The proposed approach exhibits significant advantages with respect to the mentioned common array signal processing methods (MVDR, ESPRIT, MUSIC, and BCS). Indeed, these systems require massive array antennas for achieving good performances. More recently, time-modulated arrays with a limited number of antenna elements have also been proposed for DoA estimation [58]–[61] with the goal to reduce the number of antennas and overall computational complexity. However, the hardware of the backend network is still complex, involving properly connected phase shifters, switches, and power combiners. On the contrary, the metasurface-based DoA system shifts most part of the computational efforts at the electromagnetic level, thus reducing the latency in detection and removing the need of a complex circuitry [62]. Here, both the frequency modulation and the spatial unbalancing needed for estimating the DoA are performed mainly at the metasurface level, whereas the remaining computation is extremely low cost and consists only in the evaluation of the relative difference in amplitude of the two first-order harmonics received by the fixed detecting antenna. In Sections III and IV, we describe the analytical model used for the DoA estimation and demonstrate through a proper set of numerical simulations the high accuracy reached by this method.

This article is organized as follows. After having illustrated the basic idea, in Section II, we analytically derive the temporal modulation scheme to apply to a space–time modulated metasurface for generating the two desired first-order harmonics and the spatial modulation scheme for achieving the breaking of the spatial symmetry of each order harmonic scattering pattern. In Section III, the analytical DoA estimation method based on the double-sideband (DSB) space–time modulated metasurface is derived for both 1-D and 2-D cases. In Section IV, a realistic metasurface is used for demonstrating numerically the accuracy of the proposed method for DoA estimation. Different configurations have been tested, showing the operative bounds of the proposed system. Finally, in Section V, a short conclusion of our work is given.

II. Space–Time Modulated Metasurface for DoA Estimation

In this section, we present the proposed DoA estimation method based on space–time coding modulated metasurfaces.

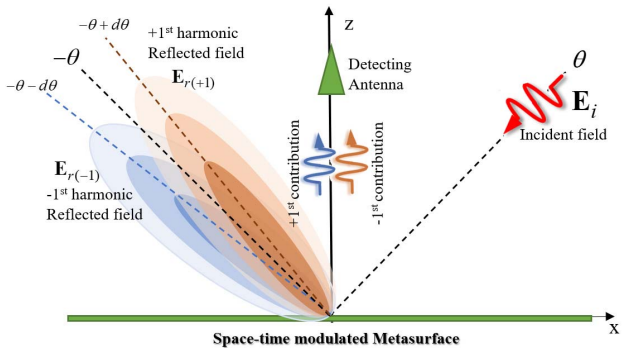

Fig. 1. Illustration of the operative scenario of a space–time modulated metasurface for DoA estimation.

After having introduced the basic idea, we analytically describe the realization of the DSB time modulation by using a 1 bit coded metasurface, which allows exciting the required $\pm$1st harmonics in reflection. The breaking of the spatial symmetry of each order harmonic scattering pattern is achieved by applying a delayed copy of the modulating signal to adjacent portions of the space–time modulated metasurface.

A. Basic Idea of DoA Estimation

Let us consider the operative scenario reported in Fig. 1. A space–time modulated metasurface is illuminated by a monochromatic plane wave at frequency ω_0 propagating with an angle θ with respect to the positive z-direction.

We assume that the metasurface-based DoA system operates only on the xz plane. This constrain will be relaxed later. Regardless the technology used for imparting the space–time modulation on the metasurface, when its surface properties are temporally modulated with frequency $\omega_p \ll \omega_0$, a frequency mixing between the incident and modulating signals takes place, spreading the energy of the incident field over a number of frequency harmonics located at $\omega_0 \pm k\omega_p$, with $k = 1, 2, 3, \ldots$ In the case of temporally modulated spatial uniform metasurfaces [20], [21], the reflected field propagates toward the specular direction $(-\theta)$. However, the metasurfaces can also be modulated in space, thus allowing the frequency contributions of the reflected field being radiated toward different directions. This allows obtaining a spatial splitting of the radiation patterns, as demonstrated by several works on space–time modulated metastructures [35], [37], [43], [52]. In Fig. 1, the radiation patterns of the two first-order harmonics at $\omega_0 \pm \omega_p$ are shown, one pointing toward $-\theta + d\theta$ and another pointing toward $-\theta - d\theta$. The detecting antennas placed in the far-field region just above the metasurface can now receive a different amplitude contribution at the two frequencies $\omega_0 \pm \omega_p$ and estimate the DoA of the incident plane wave based on the relative unbalancing of such values.

B. DSB Modulation in Time Coding Metasurfaces

The main purpose of this section is to show analytically how a time-varying reflective metasurfaces can generate the required harmonics in the reflected spectrum for applying the

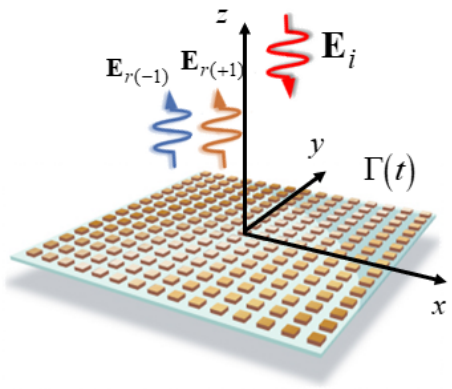

Fig. 2. DSB modulating metasurface illuminated by a normally incident plane wave able to reflect a plane wave consisting of a superposition of the two first-order harmonics.

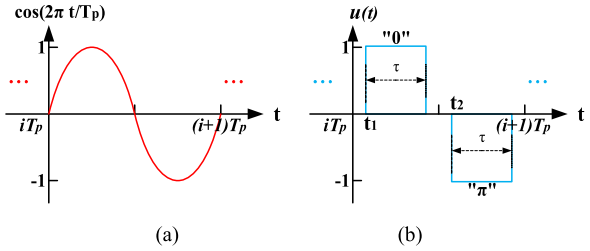

Fig. 3. (a) Temporal signal with cosine profile to be used for achieving a perfect DSB excitation at frequencies $\omega_0 \pm \omega_p$. (b) Approximate three-state signal used to match the curves in (a).

proposed method for DoA estimation. Since we are, here, interested in the temporal modulation of the incident wave, we can relax the constrain on the oblique illumination condition and assume that the metasurface is normally illuminated by the plane wave. In Sections III and IV, we will also consider the effect of the oblique incidence.

In Fig. 2, we report an ideal nonpenetrable (i.e., characterized by a zero-transmission) reflective metasurface, whose macroscopic response can be modeled through its time-varying reflection coefficient $\Gamma(t)$. The metasurface is illuminated by a normally incident plane wave of the form

$$\mathbf{E}_i(z,t) = \mathbf{E}_0 e^{jk_0 z} e^{j\omega_0 t} \tag{1}$$

and the desired reflected field consists of the superposition of the two first-order harmonics at frequencies $\omega_0 \pm \omega_p$ with the same amplitude

$$\mathbf{E}_r(z,t) = \mathbf{E}_r e^{-jk_0 z}\left[e^{j(\omega_0+\omega_p)t} + e^{j(\omega_0-\omega_p)t}\right]. \tag{2}$$

At the metasurface location, i.e., $z = 0$, the incident and reflected fields are related as follows:

$$\mathbf{E}_r(0,t) = \mathbf{E}_i(0,t) \cdot \Gamma(t) \tag{3}$$

where $\Gamma(t)$ is the degree-of-freedom we use to achieve the generation of two equal amplitude harmonics at $\omega_0 \pm \omega_p$.

Combining (1)–(3), the reflection coefficient $\Gamma(t)$ can be expanded in the form

$$\Gamma(t) = \frac{E_r}{E_0}\left(e^{j\omega_p t} + e^{-j\omega_p t}\right) = 2\frac{E_r}{E_0}\cos\omega_p t. \tag{4}$$

To satisfy the passivity constrain, in (4), the amplitude of the reflected field of each of the two first-order harmonics is half compared to the one of the incident field, i.e., $E_r = E_0/2$. This implies that half of the overall impinging energy is distributed between the two first-order harmonics at $\omega_0 \pm \omega_p$, whereas the rest is necessary dissipated by the intrinsic reflective response of the metasurface with cosine temporal profile due to the zeros of the cosine function. Despite the cosine temporal profile of the reflection coefficient theoretically ensures the required response from the metasurface, such a temporal profile needs a continuous modulation of the surface properties of the metasurface, as demonstrated in [20] and [21], which is not easy to achieve.

To simplify the metasurface implementation, the cosine temporal profile of the reflection coefficient can be approximately replaced with acceptable tolerance by a train of rectangular pulses [63], as shown in Fig. 3. The time-period T_p is the modulation period corresponding to the angular frequency $\omega_p = 2\pi/T_p$. The rectangular pulses of amplitudes "+1" and "−1" in Fig. 3(b) correspond to the reflection phases "0" or "π," respectively. Now, the start time t_1 of the "+1" state, the start time t_2 of the "−1" state, and the pulse duration τ characterizing the shape of the rectangular pulses must be analytically derived to match the cosine time profile as better as possible [63], and ensure the excitation of only the two first-order harmonics.

For the first time-period T_p starting at $t = 0$, the rectangular time sequence can be expressed as

$$u(t) = \begin{cases} +1, & t_1 \le t \le t_1 + \tau \\ -1, & t \le t \le t_2 + \tau \\ 0, & \text{others within}\left[0;\, T_p\right]. \end{cases} \tag{5}$$

The periodic time sequence is decomposed by using the Fourier series to highlight the contribution of different frequency harmonics as

$$u(t) = \sum_{h=-\infty}^{+\infty} a_h e^{jh\omega_p t}, \text{with } h = 0, \pm 1, \ldots, \pm\infty \tag{6}$$

where h is the order of the specific harmonic, and a_h is the corresponding Fourier coefficients, whose expression is evaluated as follows:

$$a_h = \frac{1}{T_p}\int_0^{T_p} u(t) e^{-jh\omega_p t} dt. \tag{7}$$

Considering the periodicity of the modulation, we can normalize the temporal axis with respect to the time-period T_p and obtain the dimensionless quantities

$$\tilde{t}_1 = t_1/T_p, \tilde{t}_2 = t_2/T_p, \tilde{\tau}_1 = \tau/T_p. \tag{8}$$

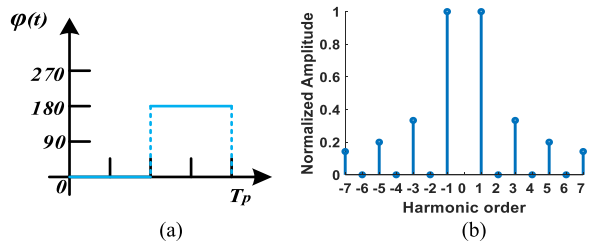

(a) (b)

Fig. 4. (a) Time-varying phase profile $\varphi(t)$ of the time sequence $u(t)$ to achieve DSB modulation. (b) Normalized coefficient amplitude of the generated harmonics.

Equation (7) can now be easily evaluated as follows:

$$\begin{aligned} a_h &= \int_0^1 u(t)e^{-j2\pi h\tilde{t}}d\tilde{t} \\ &= \left(\int_{\tilde{t}_1}^{\tilde{t}_1+\tilde{\tau}} e^{-j2\pi h\tilde{t}}d\tilde{t} - \int_{\tilde{t}_2}^{\tilde{t}_2+\tilde{\tau}} e^{-j2\pi h\tilde{t}}d\tilde{t}\right) \\ &= \begin{cases} 0, & h=0 \\ \dfrac{2j}{h\pi}\sin(h\pi\tilde{\tau})\sin[h\pi(\tilde{t}_2-\tilde{t}_1)]e^{-jh\pi(\tilde{t}_2+\tilde{t}_1+\tilde{\tau})}, & h\neq 0. \end{cases} \end{aligned} \tag{9}$$

Considering the term $\sin[h\pi(\tilde{t}_2-\tilde{t}_1)]$, when $\tilde{t}_2-\tilde{t}_1=0.5$, all the even-order harmonics vanish, i.e., $|a_h|=0$ for $h=2k, k\in\mathbb{Z}$. Moreover, considering the term $\sin(h\pi\tilde{\tau})$, setting $\tilde{\tau}=1/3$, the hth-order harmonics with $h=3$k, k$\in\mathbb{Z}$ also vanish. In this case, only few harmonics far from the $\pm$1st ones survive, e.g., the $\pm$5th, $\pm$7th, $\pm$11th, and so on. This configuration ensures the highest isolation between the first-order harmonic and the other order harmonics achievable with a binary time-modulated metasurface. However, it is worth noticing that, to exactly match the temporal profile shown in Fig. 3(b), an absorption state is required between two consecutive opposite pulses.

To further simplify the implementation, we remove the possibility to have an absorption state, setting $\tilde{\tau}=0.5$. This leads to a time-varying reflection coefficient that can exhibit only "+1" and "−1" reflection states, which corresponds to the reflection phases "0" and "π," respectively, as shown in Fig. 4(a), over a time-period T_p. Consequently, the presence of the hth-order harmonics with $h=3$k, k$\in\mathbb{Z}$, is restored. Imposing $\tilde{t}_2-\tilde{t}_1=0.5$ and $\tilde{\tau}=0.5$ into (9), the complete set of the a_h coefficients is

$$a_h = \frac{2j}{h\pi}\sin^2\left(\frac{h\pi}{2}\right)e^{-jh\pi(2\tilde{t}_1+1)}\cdot\mathrm{sgn}(h) \tag{10}$$

where sgn(h) is the sign function. In Fig. 4(b), we report the amplitude of the harmonic coefficients as a function of the harmonic order. It can be found that the amplitudes of the first-order harmonics are still three times bigger than those of the other order harmonics, letting our approach to still benefit of the presence of strong $\pm$1st-order harmonics.

In Section II-C, the required spatial modulation is imposed on the metasurface in order to achieve the splitting of the radiation patterns of the reflected 1st-order harmonics, which allows estimating the DoA of the incident wave.

C. Pattern Unbalancing in DSB-Modulated Metasurface

Once the proper temporal modulation of the 1 bit space–time metasurface is properly defined (see Section II-B for further details), the spatial asymmetry must be introduced for splitting the radiation patterns of the $\pm$1st-order harmonics and enable the DoA estimation capability of the system. The metasurface is partitioned in areas of width D in the x-direction, called sub-macrocells, each of which covers the entire extension along the y-direction, including $N_x\times N_y$ lines of space–time modulated inclusions, as shown in Fig. 5(a).

Here, the spatial asymmetry is introduced by applying different modulation signals to adjacent sub-macrocells, i.e., "Sub-macrocell 1" modulated by the signal $u_1(t)$ and "Sub-macrocell 2," modulated by the signal $u_2(t)$, reported in Fig. 5(b) and (c), respectively. The two signals are identical, except for a minor time delay Δt. They compose the DoA-MTS macro unit-cell responsible for the space–time asymmetry in the reflected patterns. It is worth mentioning that, due to the uniformity along the y-direction, the scheme in Fig. 5(a) can perform DoA estimation only for plane waves propagating on the xz plane.

Since the proposed method is valid regardless of the specific technology and subwavelength inclusion composing the metasurface, in the following, we describe its scattering pattern in terms of the array factor. The complete scattering response can easily be obtained by multiplying the array factor we derive in the following and the radiation pattern of the single subwavelength inclusion composing the metasurface [64]. The array factor of the single DoA-MTS macro unit-cell for the h-th harmonic is indicated as $af_h(\theta,\varphi)$ and can be written as the product of the array factors of the arrays of subwavelength metasurface unit-cell in the x- and y-directions

$$\begin{aligned} &af_h(\theta,\phi) \\ &= \sum_{i=1}^{2}\sum_{n_x=1}^{N_x} a_h^{(i)} e^{jk_0[(n_x-1)p_x+(i-1)D](\sin\theta\cos\phi-\sin\theta_{inc}\cos\phi_{inc})}\times \\ &\quad\times\sum_{n_y=1}^{N_y} e^{jk_0(n_y-1)p_y(\sin\theta\sin\phi-\sin\theta_{inc}\sin\phi_{inc})}. \end{aligned} \tag{11}$$

In (11), the parameters $p_{x,y}$ are the periodicities of the subwavelength inclusions in x- and y-directions, respectively, k_0 is the free-space wavevector of the incident wave, and θ_{inc},ϕ_{inc} identify the oblique incident angle of the illuminating wave.

The weighting coefficient $a_h^{(i)}$ is the complex amplitude of the hth harmonic generated by the modulated subwavelength modulated inclusions within the sub-macrocell i. With reference to Figs. 3(b) and 5(b) and (c), for identifying the starting time of the modulating signals of the two sub-macrocells, the corresponding complex amplitudes are

$$a_h^{(i)} = \begin{cases} \dfrac{2j}{h\pi}\sin^2\left(\dfrac{h\pi}{2}\right)e^{-jh\pi(2\tilde{t}_1^{(1)}+1)}\cdot\mathrm{sgn}(h), & i=1 \\ \dfrac{2j}{h\pi}\sin^2\left(\dfrac{h\pi}{2}\right)e^{-jh\pi(2\tilde{t}_1^{(2)}+1)}\cdot\mathrm{sgn}(h), & i=2. \end{cases} \tag{12}$$

In (12), when $i=1$, the complex-valued coefficient a_h is obtained for $\tilde{t}_1^{(1)}=\tilde{t}_1$, whereas, when $i=2$, the

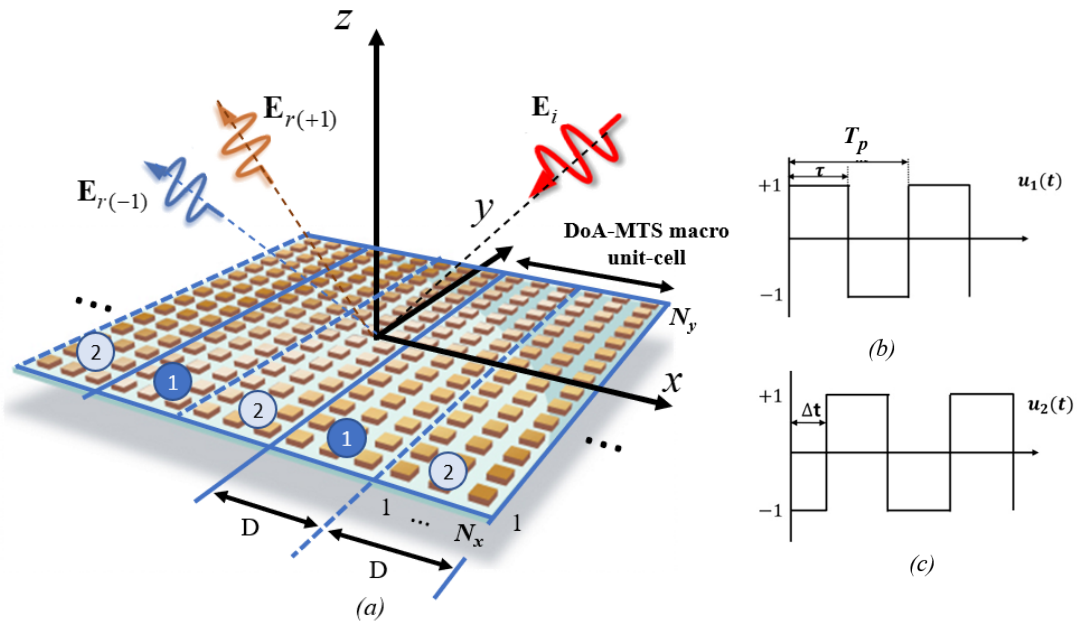

Fig. 5. (a) Sketch of the space–time modulation scheme apply to a DSB modulating metasurface illuminated by an incident plane wave able to reflect a plane wave consisting of a superposition of the two first-order harmonics. (b) and (c) Temporal signals used for modulating the two sub-macrocells composing the DoA-MTS macro unit-cell.

complex-valued coefficient a_h is obtained for $\tilde{t}_1^{(2)} = \tilde{t}_1 + \Delta\tilde{t}$, where $\Delta\tilde{t} = \Delta t/T_p$. Substituting (12) into the first double-summation term of (11), we obtain

$$\begin{aligned} af_h(\theta,\phi) = {} & \frac{2j}{h\pi}\sin^2\left(\frac{h\pi}{2}\right)e^{-jh\pi(2\tilde{t}_1^{(1)}+1)}\cdot \mathrm{sgn}(h)\times \\ & \times\left(1+e^{-j2h\pi\,\Delta\tilde{t}}e^{jk_0D(\sin\theta\cos\phi-\sin\theta_{inc}\cos\phi_{inc})}\right)\times \\ & \times\sum_{n_x=1}^{N_x}e^{jk_0(n_x-1)p_x(\sin\theta\cos\phi-\sin\theta_{inc}\cos\phi_{inc})}\times \\ & \times\sum_{n_y=1}^{N_y}e^{jk_0(n_y-1)p_y(\sin\theta\sin\phi-\sin\theta_{inc}\sin\phi_{inc})}. \end{aligned} \tag{13}$$

As shown in Fig. 5(a), the entire DoA estimating metasurface consists of many DoA-MTS macrocells, say M, and thus, the full array factor describing the scattering pattern of the entire metasurface is

$$AF_h(\theta,\varphi) = \sum_{m=1}^{M} af_h(\theta,\phi)e^{j2k_0(m-1)D(\sin\theta\cos\phi-\sin\theta_{inc}\cos\phi_{inc})} \tag{14}$$

where M is the number of DoA-MTS macrocells.

Now, we can notice an interesting term in (13) and also in (14), which allow us enabling the spatial asymmetry in the scattered patterns for the two first-order harmonics of the reflected field; depending on the value of $h = \pm 1$, identifying the upper and lower sidebands, the term $1 + e^{-j2h\pi\,\Delta\tilde{t}}e^{jk_0D(\sin\theta\cos\phi-\sin\theta_{inc}\cos\phi_{inc})}$ exhibits two different values in the complex exponential, which unbalances the scattering pattern around the direction $[-\theta_{inc}; -\phi_{inc}]$.

III. Metasurface-Based DoA Estimation Method

A. 1-D DoA Estimation Method Based on DSB Metasurface

Let us start deriving the DoA estimation equations in the case of illuminating plane waves, whose wavevectors lie on the xz plane, i.e., $\phi_{inc} = 0$. The goal is to estimate the performances of the proposed system in identifying the angle θ_{inc} of the incident plane wave, i.e., 1-D DoA estimation.

In this scenario, the uniformity along the y-direction relaxes the need to consider the other scattering directions besides the ones laying on the xz plane. Thus, setting $\phi = 0$ and observing the metasurface in broadside ($\theta = 0$), where the detecting antenna is located, the amplitude ratio between $AF_{-1}(\theta_{inc}, \phi = 0)$ and $AF_{+1}(\theta_{inc}, \phi = 0)$ can be written as

$$\begin{aligned} \left|\frac{AF_{-1}}{AF_{+1}}\right| = \left|\frac{af_{-1}}{af_{+1}}\right| &= \left|\frac{1+e^{+j2\pi\,\Delta\tilde{t}}e^{jk_0D\sin\theta_{inc}}}{1+e^{-j2\pi\,\Delta\tilde{t}}e^{jk_0D\sin\theta_{inc}}}\right| = \\ &= \frac{\sqrt{1+\cos(k_0D\sin\theta_{inc}+2\pi\,\Delta\tilde{t})}}{\sqrt{1+\cos(k_0D\sin\theta_{inc}-2\pi\,\Delta\tilde{t})}} \\ &= \frac{\left|\cos\left(\frac{1}{2}k_0D\sin\theta_{inc}+\pi\,\Delta\tilde{t}\right)\right|}{\left|\cos\left(\frac{1}{2}k_0D\sin\theta_{inc}-\pi\,\Delta\tilde{t}\right)\right|}. \end{aligned} \tag{15}$$

Using trigonometric angle sum and difference identities to expand the right-hand side of (15), it can be simplified to obtain the DoA estimation curve as

$$\begin{aligned} g(f(\theta_{inc})) &= \tan\left(\frac{1}{2}k_0D\sin\theta_{inc}\right) \\ &= \frac{|AF_1|-|AF_{-1}|}{|AF_1|+|AF_{-1}|}\frac{\cos(\pi\,\Delta\tilde{t})}{\sin(\pi\,\Delta\tilde{t})} \end{aligned} \tag{16}$$

from which, we can estimate the DoA angle θ_{inc} as

$$\theta_{inc} = g^{-1}(f^{-1}(\theta_{inc})) = \\ = \text{arcSin}\left(\frac{2}{k_0 D}\text{arcTan}\left(\frac{|AF_1| - |AF_{-1}|}{|AF_1| + |AF_{-1}|}\frac{\cos(\pi\,\Delta\tilde{t})}{\sin(\pi\,\Delta\tilde{t})}\right)\right). \tag{17}$$

To avoid angle ambiguity when (17) is used for DoA estimation, the curve should be monotonic among the estimation range; thus, the conditions for no angle ambiguity are expressed as

$$-\frac{\pi}{2} \le \frac{1}{2}k_0 D\sin\theta_{inc} \pm \pi\,\Delta\tilde{t} \le \frac{\pi}{2}. \tag{18}$$

In the range of direction estimation $\theta_{inc} \in [0;\pi/2]$, the sine function $\sin\theta_{inc}$ is real and within $[0;+1]$. Substituting $k_0 = 2\pi/\lambda_0$ into (18), to avoid angle ambiguity, the conditions can be written as

$$\left|\Delta\tilde{t}\right| \le \frac{1}{2} - \frac{D}{\lambda_0}. \tag{19}$$

Equation (19) defines a bound for the time delay between the modulating signals to be applied for a given electrical dimension D/λ_0 of the sub-macrocell. However, it is worth remembering that due to the periodicity of the modulating signals $u_2(t)$, the time delay is always within a period, i.e., $|\Delta\tilde{t}| \le 1/2$. This sets also an upper bound for the sub-microcell dimension D that cannot exceed the half-a-wavelength width.

As to chromatic plane waves, the proposed approach is still effective as long as the bandwidth B of the incident signal is smaller than the modulation frequency $f_p = 1/T_p$ ($f_p < \text{B}$). If $f_p \ge \text{B}$, the harmonic spectra will not overlap, and thus, we can use the harmonic bands to estimate the DoA like in the case of the monochromatic incident wave. Though theoretically f_p can be large enough to obtain wideband DoA estimation, due to hardware limitation, in the performed experiments [45], f_p can reach only the MHz. For practical linear frequency modulation (LFM), incident waves ($f_p < \text{B}$), in [59], the LFM signal with long duration can be separated into multiple short durations, and the bandwidth of each short duration is smaller than the modulation frequency. This avoids overlapping and relaxes the limitation of LFM bandwidth. In [60], the pulse compression technology is used to calculate the modulation harmonics, and the harmonic coefficients of the modulated signals can also be obtained by the output of the matched filter.

B. 2-D DoA Estimation Extension

The above method can also be extended to 2-D DoA estimation. The 2-D detection scheme requires that the scattering pattern splitting of the 1st-order harmonics of the reflected field is introduced for both x- and y-directions of the metasurface to estimate both polar coordinates $[\theta_{inc};\phi_{inc}]$. This can be obtained by modulating the metasurfaces separately along the two main axes, x- and y-directions. For example, the 1-D modulation scheme reported in Section II-C can be applied in sequence along the x- and y-directions by properly controlling in real time the modulation profile on the metasurface or, alternatively, it is possible to use two identical DoA metasurfaces arranged orthogonally, as shown in Fig. 6.

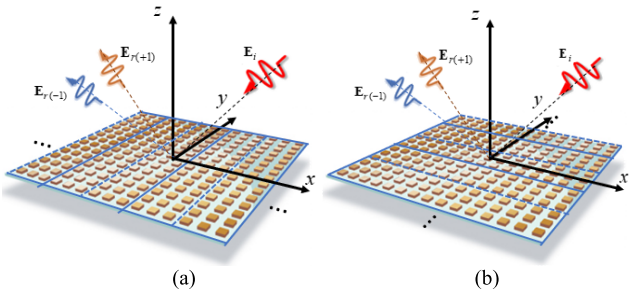

Fig. 6. 2-D DoA estimation arrays: (a) first array along the x-direction and (b) second array along the y-direction.

Following the same procedure illustrated in Section III-A for the 1-D DoA estimation, we can derive the estimating function for the spatial modulation along the x-direction [Fig. 6(a)] considering an incident plane wave impinging from the direction $[\theta_{inc};\phi_{inc}]$. Being the detection direction $\theta = \varphi = 0$, where the detecting antenna is located, we can write

$$g_x(f_x(\theta_{inc},\varphi_{inc})) = \tan\left(\frac{1}{2}k_0 D\sin\theta_{inc}\cos\varphi_{inc}\right) \\ = \frac{|AF_{1x}| - |AF_{-1x}|}{|AF_{1x}| + |AF_{-1x}|}\frac{\cos(\pi\,\Delta\tilde{t})}{\sin(\pi\,\Delta\tilde{t})} \tag{20}$$

that returns

$$\sin\theta_{inc}\cos\varphi_{inc} = \frac{2}{k_0 D}\arctan\left(\frac{|AF_{1x}| - |AF_{-1x}|}{|AF_{1x}| + |AF_{-1x}|}\frac{\cos(\pi\,\Delta\tilde{t})}{\sin(\pi\,\Delta\tilde{t})}\right). \tag{21}$$

Moreover, the estimating function for the spatial modulation along the y-direction [Fig. 6(b)] is

$$g_y(f_y(\theta_{inc},\varphi_{inc})) = \tan\left(\frac{k_0 D\sin\theta_{inc}\sin\varphi_{inc}}{2}\right) = \\ = \frac{|AF_{1y}| - |AF_{-1y}|}{|AF_{1y}| + |AF_{-1y}|}\frac{\cos(\pi\,\Delta\tilde{t})}{\sin(\pi\,\Delta\tilde{t})} \tag{22}$$

that, in turn, returns

$$\sin\theta_{inc}\sin\varphi_{inc} = \frac{2}{k_0 D}\arctan\left(\frac{|AF_{1y}| - |AF_{-1y}|}{|AF_{1y}| + |AF_{-1y}|}\frac{\cos(\pi\,\Delta\tilde{t})}{\sin(\pi\,\Delta\tilde{t})}\right). \tag{23}$$

From (21) and (23), θ_{inc} and ϕ_{inc} can be derived in the closed form as

$$\varphi_{inc} = \arctan\left[\frac{\arctan\left(\frac{|AF_{1x}|-|AF_{-1x}|}{|AF_{1x}|+|AF_{-1x}|}\frac{\cos(\pi\,\Delta\tilde{t})}{\sin(\pi\,\Delta\tilde{t})}\right)}{\arctan\left(\frac{|AF_{1y}|-|AF_{-1y}|}{|AF_{1y}|+|AF_{-1y}|}\frac{\cos(\pi\,\Delta\tilde{t})}{\sin(\pi\,\Delta\tilde{t})}\right)}\right] \tag{24}$$

$$\theta_{inc} = \arcsin \\ \left[\frac{2}{k_0 D\cos\phi_{inc}}\arctan\left(\frac{|AF_{1x}| - |AF_{-1x}|}{|AF_{1x}| + |AF_{-1x}|}\frac{\cos(\pi\,\Delta\tilde{t})}{\sin(\pi\,\Delta\tilde{t})}\right)\right]. \tag{25}$$

The 2-D DoA estimation results can be expressed as (26); when θ is positive, $\theta = \theta$, $\phi = \phi$, but if θ is negative,

$$\theta = -\theta,\ \phi = \phi + \pi$$

$$(\theta, \phi) = \begin{cases} (\theta, \phi), & \theta > 0 \\ (-\theta, \phi + \pi), & \theta < 0. \end{cases} \tag{26}$$

C. Accuracy of the DoA Estimation Method

In this section, the DoA estimation accuracy is evaluated using the estimation formulas of the incidence angles $[\theta_{inc}; \phi_{inc}]$ derived in Sections III-A and III-B. A Monte Carlo simulation is used to analyze the estimation accuracy, when the received signals have certain noise. This numerical simulation investigates the mean square error (MSE) between the estimated and actual direction of incidence for the 1-D DoA case. The accuracy of the proposed method is linked to the slope of the DoA estimation curve. When the noise induces the same level error to $g(f(\theta_{inc}))$, the range of retrieved θ_{inc} is dependent on the slope of the DoA estimation curve. That is to say if the slope is steeper, the retrieved range is smaller and DoA estimation is more accurate. On the contrary, if the slope is flatter, the retrieved range is wider and the accuracy becomes lower. A plane wave at frequency $f_0 = 3.3$ GHz illuminates the metasurface in the xz plane ($\phi_{inc} = 0°$) with different incident angles, ranging from $\theta_{inc} = -80°$ to $\theta_{inc} = +80°$, with a step of 5°. The DoA space–time modulated metasurface consists of only one DoA-MTS macrocell, composed, in turn, by two sub-microcells with $D = 0.44\lambda_0$ and the time delay fraction $\Delta\tilde{t} = 0.05T_p$. The modulation frequency is $f_p = 1$ MHz and sampling frequency $f_s = 10$ GHz. The signal-to-noise ratio (SNR) is set as 10 dB with respect to the amplitude of the total reflective field from the metasurface. For each incident angle, a 1000-times Monte Carlo simulation is used to calculate the MSE of the estimation. The simulation results are shown in Fig. 7(a), where it can be found that the error is lower than 0.4° over the entire field of view. Much lower error is found near ±60°, whereas relative larger errors are found near 0°, ±90°, due to the changes of the slope of the estimation curve as explained above in Fig. 7(b).

Here, the accuracy of the DoA estimation is discussed by comparing the proposed method and the conventional MUSIC algorithm. To keep the same conditions of the Monte Carlo simulation, we use the same array size, center frequency, sampling frequency, SNR, etc. In the MUSIC method [12] with two omnidirectional antennas (dimensions $2 \times 0.44\lambda$), 5000 continuous data points of time-domain far field are sampled from each antenna. In the MUSIC method, thus, 10 000 (5000 × 2) data points are sampled in total. In the proposed method, the modulation frequency is set as $f_p = 1$ MHz, and 10 000 data points are sampled per modulation period. The MSEs of the proposed and MUSIC methods are plotted in Fig. 7(a). Comparable accuracy levels are achieved.

IV. DoA Estimation Using a Realistic Space–Time Modulated Metasurface

To validate the proposed method based on a space–time modulated metasurface, a realistic metasurface structure is, here, considered and properly modulated for achieving the excitation of the ±1st-order harmonics and the splitting of their scattering patterns. The metasurface should be able to exhibit unitary amplitude and a binary 0–π phase of the reflection coefficient over a field of view as wide as possible.

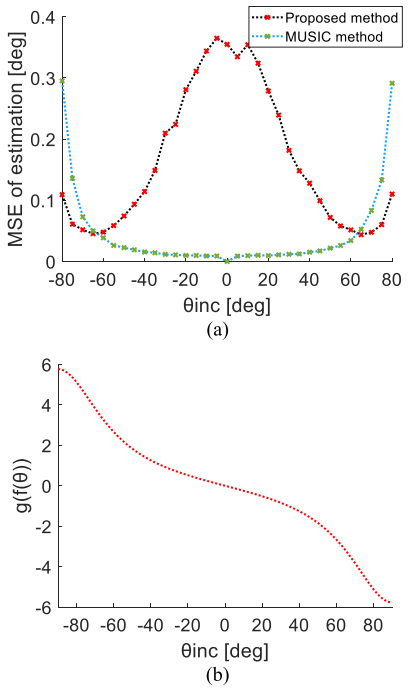

Fig. 7. (a) Comparison of MSEs with MUSIC method. (b) Corresponding analytical DoA estimation curve of the proposed method by two sub-microcells with $D = 0.44\lambda_0$.

In Fig. 8(a) and (b), a single-polarized inclusion is proposed, which consists of adjacent patches placed on top of a Rogers 3010 ($\varepsilon_r \approx 10.2$) dielectric substrate and connected through p-i-n diodes (BAR 65-03W) [65], which has two operational states, ON and OFF, controlled by a bias voltage (3.3 or 0 V). The dimensions of the unit-cell hosting the inclusion are $p_x = 10$ mm and $p_y = 10$ mm, the height is $h_s = 5.2$ mm, and other parameters are $w_1 = 1.59$ mm, $l1 = 3.5$ mm, $w2 = 0.5$ mm, and $l2 = 1$ mm.

To show the 1 bit phase performance of the designed unit-cell under different operation states of the p-i-n diodes, we perform the full-wave simulation with CST Studio Suite [66]. In our simulation, when the p-i-n diode is at the ON-state, it can be equivalent as a series circuit of parasitic inductance (1.61 nH) and resistance (0.7 Ω); if the p-i-n diode is at the OFF-state, a series circuit of parasitic inductance (1.39 nH), capacitance (0.41 pF), and resistance (1.41 Ω) is used to describe the physical model. In addition, a Floquet port is used to produce y-polarized waves incident onto the meta-atom and receive the reflected waves. Periodic boundary condition is set to its four sides to model the infinite array. It exhibits the binary 0–π phase response at 3.3 GHz, with a reflection amplitude larger than 0.82 over the angular range [0°–70°] of the incident angles [Fig. 8(c) and (d)].

A. 1-D DoA Estimation Using Different Widths of the DoA Macrocell

To demonstrate the DoA estimation using the proposed DSB space–time modulated metasurface, a simulation is

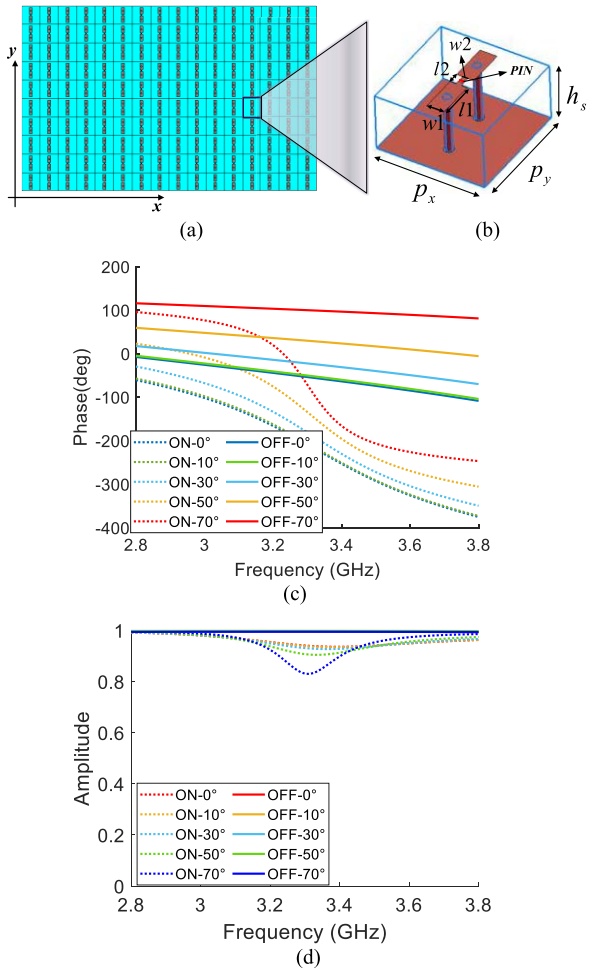

Fig. 8. Binary metasurface and the reflection response of the unit-cell: (a) sketch of the metasurface composed of 10 × 16 unit-cells; (b) geometry of the 1 bit unit-cell; (c) reflection phase; and (d) reflection amplitude of the unit-cell as a function of frequency for the two states "0" and "π," under different illumination directions.

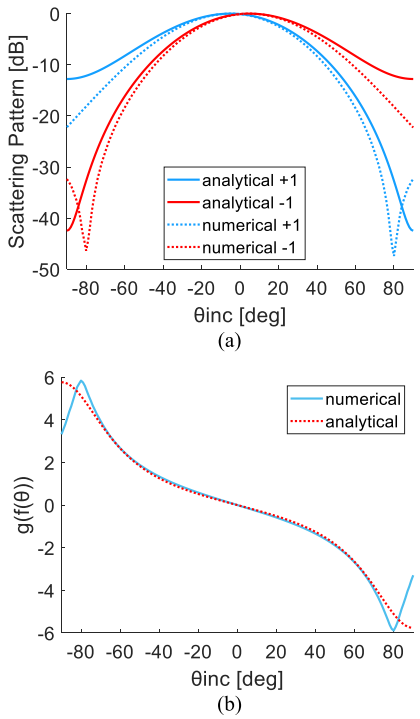

Fig. 9. (a) Normalized scattering patterns of +1- and −1-order harmonics for the DoA estimation: comparison between analytical and numerical with the $[-90°, 90°]$ estimation range. (b) Corresponding DoA estimation curve, when array is 10 × 8 and $N_x = 4$.

TABLE I
$N_x = 4$, DoA Estimation Results

Direction [deg]	Estimation [deg]	Abs. Error [deg]
0	0.01	0.01
+10	11.39	1.39
+20	21.65	1.65
+30	31.74	1.74
+40	41.47	1.47
+50	50.65	0.65
+60	59.85	0.15
+70	70.26	0.26
-10	-11.15	1.15
-20	-21.46	1.46
-30	31.81	1.81
-40	41.52	1.52
-50	-50.64	0.64
-60	-59.69	0.31
-70	-70.23	0.23

implemented considering a metasurface with one DoA-MTS microcell, composed by two sub-macrocells, each of which including $N_x = 4$ and $N_y = 10$ unit-cells shown in Fig. 8(b) along the x- and y-directions, respectively. The operative central frequency is $f_0 = 3.3$ GHz, and the modulation frequency is $f_m = 1$ MHz.

At the operative frequency, the periodicity of the 1 bit unit-cell along both axes is $p_{x,y} = 0.11\lambda_0$. According to the upper-bound limit defined in (19), the time delay Δt between the modulating signals $u_1(t)$ and $u_2(t)$ must satisfy the relation $\Delta t \leq (0.5 - N_x p_x/\lambda_0)T_p = 0.06T_p$. Here, the time delay has been, thus, set at $\Delta t = 0.05T_p$.

The normalized scattering patterns of +1st- and −1st-order harmonics are shown in Fig. 9(a), and the DoA estimation curve can be calculated from (16) by the scattering patterns of +1st- and −1st-order harmonics. In Fig. 9(b), we show that the analytical and numerical curves agree very well except for the boundary of the incident angle range.

The DoA estimation results are summarized in Table I, where it is worth noticing that the proposed method returns very small absolute errors within the range $[-70°, 70°]$ between actual and estimated DoA. The other directions, out of this range, return a wrong estimation, due to the deterioration of the phase/amplitude responses of the unit-cell and the coupling effects among the unit-cells.

Also, it is interesting to consider a narrower field of view and derive the corresponding modifications to the modulation scheme at the metasurface level. For example, limiting the field of view to the range $[-30°, 30°]$, using (19), we obtain that DoA estimation can be done using a larger width of the sub-macrocell. In particular, using again $\Delta t = 0.05T_p$, the width D can be doubled, thus allowing to include $N_x = 8$ unit-cells along the x-direction and $N_y = 10$ unit-cells along

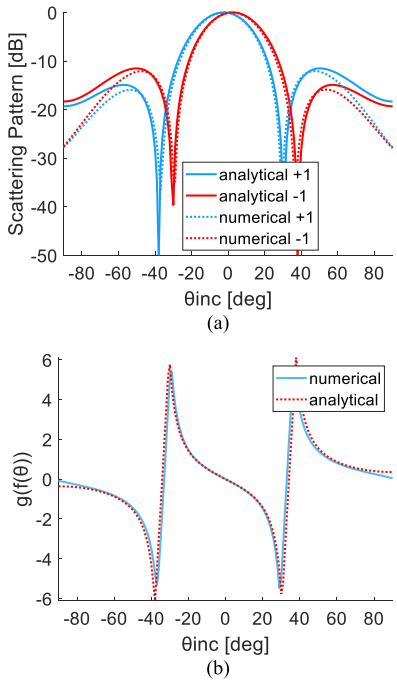

Fig. 10. (a) Normalized scattering patterns of +1- and −1-order harmonics for the DoA estimation: comparison between analytical and numerical with the $[-30°, 30°]$ estimation range. (b) Corresponding DoA estimation curve when array is 10×16 and $N_x = 8$.

TABLE II

$N_x = 8$, DoA Estimation Results

Direction [deg]	Estimation [deg]	Abs. Error [deg]
0	0.05	0.05
+10	9.83	0.17
+20	20.25	0.25
+30	29.35	0.65
-10	-9.80	0.20
-20	-20.29	0.29
-30	29.37	0.63

the y-direction within a single sub-microcell. Therefore, the metasurface is composed by 10×16 unit-cells.

The normalized scattering patterns of +1st- and −1st-order harmonics and the DoA estimation curve are reported in Fig. 10. In the angular range of interest, the curve is monotonic and single-valued, but it is steeper than the one in Fig. 9(b). This implies an enhancement of the estimation accuracy, as shown in Table II.

In practical implementation, there are two ideas to reduce the blockage effect of the receiving antenna: 1) miniaturize the detecting antenna to reduce the aperture and 2) place the detecting antenna with a certain offset angle [67], to reduce the blockage to the incident wave from the angles we are interested in. Moreover, 1 bit refracting time-modulated metasurface can be introduced to implement the proposed method to avoid the occlusion effect [68].

B. 1-D DoA Estimation Using Different Time Delays

According to (16), the DoA estimation curve is related not only to the dimensions of the DoA element, but also to the time delay Δt of the modulating signals $u_1(t)$ and $u_2(t)$ applied to the two sub-macrocells of the DoA-MTS microcell. To demonstrate the impact of the time delay in the DoA estimation accuracy, a simulation is implemented considering a metasurface composed by just one DoA-MTS microcell, whose sub-microcells include $N_x = 4$ and $N_y = 10$ unit-cells along the x- and y-directions, respectively.

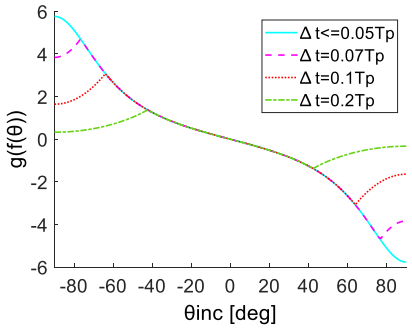

Fig. 11. DoA estimation curves with different time delays, when array is 10×8 and $N_x = 4$.

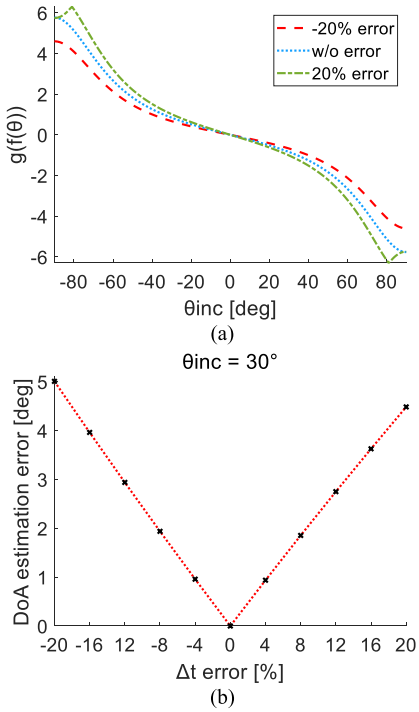

Fig. 12. When array is 10×8 and $N_x = 4$: (a) DoA estimation curves with error of time delays and (b) DoA estimation error due to time delay error, $\theta_{\text{inc}} = 30°$.

In Fig. 11, we report the DoA estimation curves for different time delays Δt. The light blue curve represents all the results for any value of $\Delta t \leq 0.05T_p$ that satisfies (19). In this case, the curve is monotonic, and there is no ambiguity on the DoA. On the contrary for larger time delays (dashed curves in Fig. 11), the operational field of view shrinks according to (19), where the angle θ must be smaller for satisfying the constrain.

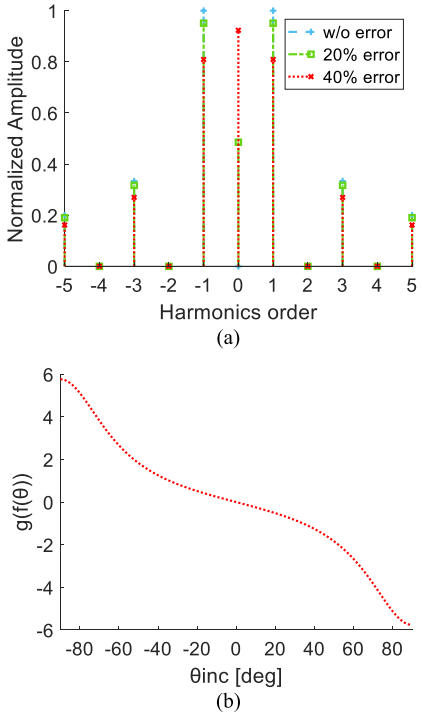

Fig. 13. (a) Normalized spectrums of 1 bit temporal modulation with different phase errors. (b) Corresponding DoA estimation curve maintains unchanged when array is 10×8 and $N_x = 4$.

The DoA estimation accuracy is obviously affected by the error in time delays, being this quantity vitally important to the accuracy of the presented method. To analyze the effect of potential errors on time delays, here, we consider the delay of periodic temporal modulations as $\Delta t = 0.05T_p$, whose corresponding DoA estimation curve is shown in Fig. 12(a) (blue dotted line). If there are errors in time delays within the range of $\pm 20\%$, i.e., between $\Delta t = 0.04T_p$ (Δt error is -20%) and $\Delta t = 0.06T_p$ (Δt error is 20%), the corresponding estimation curves shown in Fig. 12(a) are modified, with an incorrect range and slope of the DoA estimation curve. This will cause an error in the DoA estimation, correspondingly. For example, when $\theta_{\text{inc}} = 30°$, the DoA estimation error due to the Δt error is shown in Fig. 12(b). As expected, the DoA estimation error increases with the Δt error.

C. Analysis of 1-D DoA Estimation Error Due to Phase Error

For (17), which is derived from (13) and (15) under the condition of two ± 1 harmonics exhibiting an identical amplitude, we just use ± 1 harmonics from the spectrum to achieve the DoA estimation. Equation (17) is still suitable for modulation methods with ± 1 harmonics of identical amplitude. Different temporal modulations just affect the purity of ± 1 harmonics that we substitute into (17) but have no influence on the accuracy of DoA estimation theoretically. As shown in Fig. 13, when 1 bit temporal modulation [see Fig. 4(a)] has different phase errors, the ± 1 harmonics have identical amplitude but with different efficiencies. The DoA estimation curves keep unchanged, namely, the phase errors of 1 bit have theoretically no influence on the accuracy of the DoA estimation. When increasing the phase errors, the efficiencies of the ± 1 harmonics decrease, and the antinoise ability decreases correspondingly.

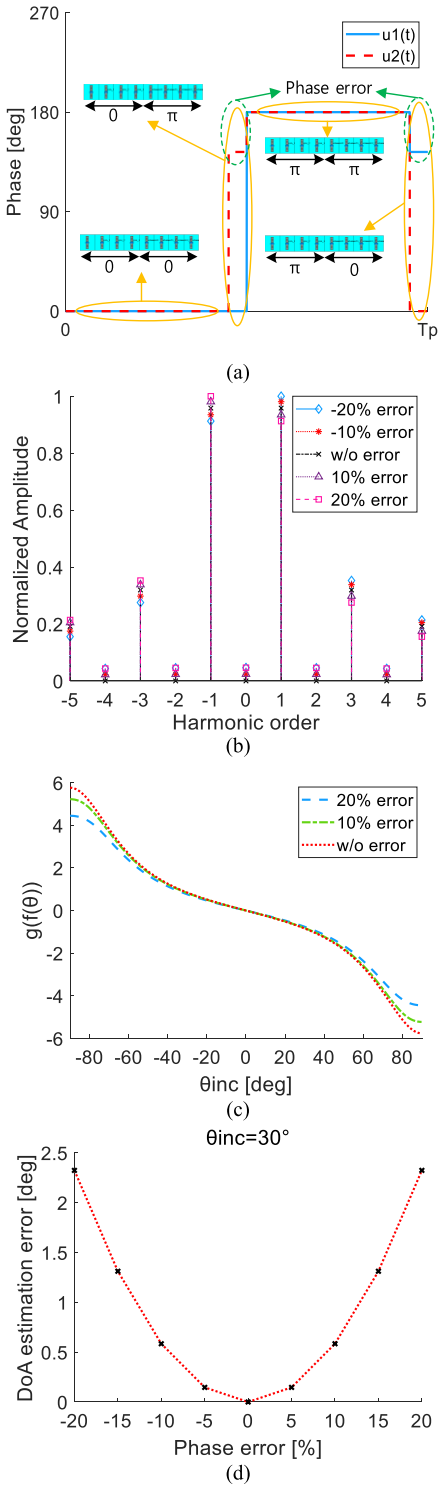

Fig. 14. (a) Time-varying phase profile of the time sequence $u_1(t)$ and $u_2(t)$, and phase errors are generated during the time delay. (b) Normalized spectrums of the generated harmonics with different phase errors. (c) Corresponding DoA estimation curves. (d) DoA estimation error due to phase error, $\theta_{\text{inc}} = 30°$.

Please note that the DoA estimation method still works when the modulation generates two ± 1 harmonics with different amplitudes. However, in this case, (15) and (17) must be rederived starting from (13) that must take into account the new modulation scheme. To better clarify this point, let us consider a modulation scheme that introduces a phase error generated during the time delay between $u_1(t)$ and $u_2(t)$, because of different boundary conditions of the sub-macrocells [as shown in Fig. 14(a)]. This error will lead to a different amplitude of ± 1 harmonics, as shown in Fig. 14(b). The corresponding DoA estimation curves are shown in Fig. 14(c), thus clearly demonstrating that they do not overlap anymore, leading to an error in the estimation. In particular, when $\theta_{\text{inc}} = 30°$, the DoA estimation error due to phase error during the time delay is shown in Fig. 14(d). Obviously, the DoA estimation error increases with the phase error.

V. Conclusion

In this article, we have proposed a DoA estimation method based on space–time modulated metasurfaces that exploits their capabilities to generate several harmonics in the scattered field, each of which is radiated toward different directions. By detecting the field in the broadside direction by using a single receiving antenna, the metasurfaces-based DoA system can estimate in real time the impinging angle of an illuminating monochromatic plane wave. The proposed approach exploits the amplitude unbalance of the received fields at broadside at only the two first-order harmonic frequencies generated by the interaction between the incident plane wave and the modulated metasurface. The analytical model for estimating the incident angle has been presented and successfully used in combination with a realistic 1 bit reflective metasurface. The accuracy of 1-D DoA estimation is verified through full-wave numerical simulations. Compared to conventional DoA estimation methods, the proposed one simplifies the computation and hardware complexity, ensuring a very good estimation accuracy. The proposed approach may have potential applications in wireless communications, target recognition, and identification.

References

[1] H. Krim and M. Viberg, "Two decades of array signal processing research: The parametric approach," *IEEE Signal Process. Mag.*, vol. 13, no. 4, pp. 67–94, Jul. 1996.

[2] H. L. Van Trees, *Detection, Estimation, and Modulation Theory, Part IV: Optimum Array Processing*. New York, NY, USA: Wiley, 2002.

[3] H. Bayer, A. Krauss, T. Zaiczek, R. Stephan, O. Enge-Rosenblatt, and M. A. Hein, "Ka-band user terminal antennas for satellite communications [antenna applications corner]," *IEEE Antennas Propag. Mag.*, vol. 58, no. 1, pp. 76–88, Feb. 2016.

[4] A. Kuchar, M. Tangemann, and E. Bonek, "A real-time DOA-based smart antenna processor," *IEEE Trans. Veh. Technol.*, vol. 51, no. 6, pp. 1279–1293, Nov. 2002.

[5] M. Burtowy, M. Rzymowski, and L. Kulas, "Low-profile ESPAR antenna for RSS-based DoA estimation in IoT applications," *IEEE Access*, vol. 7, pp. 17403–17411, 2019.

[6] M. Koivisto *et al.*, "Joint device positioning and clock synchronization in 5G ultra-dense networks," *IEEE Trans. Wireless Commun.*, vol. 16, no. 5, pp. 2866–2881, May 2017.

[7] B. Liao and S. C. Chan, "Direction finding with partly calibrated uniform linear arrays," *IEEE Trans. Antennas Propag.*, vol. 60, no. 2, pp. 922–929, Feb. 2012.

[8] R. Zhou, H. Zhang, and H. Xin, "Improved two-antenna direction finding inspired by human ears," *IEEE Trans. Antennas Propag.*, vol. 59, no. 7, pp. 2691–2697, Jul. 2011.

[9] H. Cox, R. Zeskind, and M. Owen, "Robust adaptive beamforming," *IEEE Trans. Acoust., Speech, Signal Process.*, vol. ASSP-35, no. 10, pp. 1365–1376, Oct. 1987.

[10] R. Roy and T. Kailath, "Esprit—Estimation of signal parameters via rotational invariance techniques," *IEEE Trans. Acoust., Speech, Signal Process.*, vol. 37, no. 7, pp. 984–995, Jul. 1989.

[11] J. Steinwandt, F. Roemer, and M. Haardt, "Generalized least squares for ESPRIT-type direction of arrival estimation," *IEEE Signal Process. Lett.*, vol. 24, no. 11, pp. 1681–1685, Nov. 2017.

[12] R. Schmidt, "Multiple emitter location and signal parameter estimation," *IEEE Trans. Antennas Propag.*, vol. AP-34, no. 3, pp. 276–280, Mar. 1986.

[13] D. Kundu, "Modified MUSIC algorithm for estimating DOA of signals," *Signal Process.*, vol. 48, no. 1, pp. 85–90, 1996.

[14] P. Rocca, M. A. Hannan, M. Salucci, and A. Massa, "Single-snapshot DoA estimation in array antennas with mutual coupling through a multiscaling BCS strategy," *IEEE Trans. Antennas Propag.*, vol. 65, no. 6, pp. 3203–3213, Jun. 2017.

[15] Y. Ra'di, V. S. Asadchy, and S. A. Tretyakov, "Tailoring reflections from thin composite metamirrors," *IEEE Trans. Antennas Propag.*, vol. 62, no. 7, pp. 3749–3760, Jul. 2014.

[16] V. S. Asadchy, M. Albooyeh, S. N. Tcvetkova, A. Díaz-Rubio, Y. Ra'di, and S. A. Tretyakov, "Perfect control of reflection and refraction using spatially dispersive metasurfaces," *Phys. Rev. B, Condens. Matter*, vol. 94, no. 7, Aug. 2016m Art. no. 075142.

[17] V. G. Ataloglou and G. V. Eleftheriades, "Arbitrary wave transformations with Huygens' metasurfaces through surface-wave optimization," *IEEE Antennas Wireless Propag. Lett.*, vol. 20, no. 9, pp. 1750–1754, Sep. 2021.

[18] A. Epstein and G. V. Eleftheriades, "Huygens' metasurfaces via the equivalence principle: Design and applications," *J. Opt. Soc. Amer. B, Opt. Phys.*, vol. 33, no. 2, p. A31, Feb. 2016.

[19] D. Ramaccia, D. L. Sounas, A. V. Marini, A. Toscano, and F. Bilotti, "Electromagnetic isolation induced by time-varying metasurfaces: Nonreciprocal Bragg grating," *IEEE Antennas Wireless Propag. Lett.*, vol. 19, no. 11, pp. 1886–1890, Nov. 2020.

[20] D. Ramaccia, D. Sounas, A. Alu, A. Toscano, and F. Bilotti, "Phase-induced frequency conversion and Doppler effect with time-modulated metasurfaces," *IEEE Trans. Antennas Propag.*, vol. 68, no. 3, pp. 1607–1617, Mar. 2020.

[21] Z. Wu and A. Grbic, "Serrodyne frequency translation using time-modulated metasurfaces," *IEEE Trans. Antennas Propag.*, vol. 68, no. 3, pp. 1599–1606, Mar. 2020.

[22] M. Liu, D. A. Powell, Y. Zarate, and I. V. Shadrivov, "Huygens' metadevices for parametric waves," *Phys. Rev. X*, vol. 8, no. 3, Sep. 2018, Art. no. 031077.

[23] S. B. Glybovski, S. A. Tretyakov, P. A. Belov, Y. S. Kivshar, and C. R. Simovski, "Metasurfaces: From microwaves to visible," *Phys. Rep.*, vol. 634, pp. 1–72, Apr. 2016.

[24] D. Ramaccia, S. Arcieri, A. Toscano, and F. Bilotti, "Core-shell super-spherical nanoparticles for LSPR-based sensing platforms," *IEEE J. Sel. Topics Quantum Electron.*, vol. 23, no. 2, pp. 380–387, Mar. 2017.

[25] D. Ramaccia, A. Toscano, and F. Bilotti, "Scattering and absorption from super-spherical nanoparticles: Analysis and design for transparent displays [invited]," *J. Opt. Soc. Amer. B, Opt. Phys.*, vol. 34, no. 7, p. D62, Jul. 2017.

[26] S. Vellucci, A. Monti, M. Barbuto, A. Toscano, and F. Bilotti, "Waveform-selective mantle cloaks for intelligent antennas," *IEEE Trans. Antennas Propag.*, vol. 68, no. 3, pp. 1717–1725, Mar. 2020.

[27] C. Huang, B. Sun, W. Pan, J. Cui, X. Wu, and X. Luo, "Dynamical beam manipulation based on 2-bit digitally-controlled coding metasurface," *Sci. Rep.*, vol. 7, no. 1, pp. 1–8, Feb. 2017.

[28] L. Li *et al.*, "Electromagnetic reprogrammable coding-metasurface holograms," *Nature Commu.*, vol. 8, no. 1, pp. 1–7, 2017.

[29] K. Chen *et al.*, "A reconfigurable active Huygens' metalens," *Adv. Mater.*, vol. 29, no. 17, May 2017, Art. no. 1606422.

[30] W. Tang *et al.*, "Programmable metasurface-based RF chain-free 8 PSK wireless transmitter," *Electron. Lett.*, vol. 55, no. 7, pp. 417–420, Apr. 2019.

[31] F. Monticone and A. Alù, "Metamaterial, plasmonic and nanophotonic devices," *Rep. Prog. Phys.*, vol. 80, no. 3, Mar. 2017, Art. no. 036401.

[32] L. Cong, P. Pitchappa, C. Lee, and R. Singh, "Active phase transition via loss engineering in a terahertz MEMS metamaterial," *Adv. Mater.*, vol. 29, no. 26, Jul. 2017, Art. no. 1700733.
[33] Z. Miao *et al.*, "Widely tunable terahertz phase modulation with gate-controlled graphene metasurfaces," *Phys. Rev. X*, vol. 5, no. 4, Nov. 2015, Art. no. 041027.
[34] B. Wei *et al.*, "Generating switchable and reconfigurable optical vortices via photopatterning of liquid crystals," *Adv. Mater.*, vol. 26, no. 10, pp. 1590–1595, Mar. 2014.
[35] L. Zhang *et al.*, "Space-time-coding digital metasurfaces," *Nat. Commun.*, vol. 9, no. 1, pp. 1–11, Oct. 2018.
[36] Z. Wu, C. Scarborough, and A. Grbic, "Space-time-modulated metasurfaces with spatial discretization: Free-space N-path systems," *Phys. Rev. Appl.*, vol. 14, no. 6, Dec. 2020, Art. no. 064060.
[37] X. Fang, M. Li, D. Ding, F. Bilotti, and R. Chen, "Design of in-phase and quadrature two paths space-time-modulated metasurfaces," *IEEE Trans. Antennas Propag.*, early access, Jan. 28, 2022, doi: 10.1109/TAP.2022.3145480.
[38] D. Ramaccia, A. Toscano, and F. Bilotti, "Light propagation through metamaterial temporal slabs: Reflection, refraction, and special cases," *Opt. Lett.*, vol. 45, no. 20, p. 5836, 2020.
[39] D. Ramaccia, A. Alù, A. Toscano, and F. Bilotti, "Temporal multilayer structures for designing higher-order transfer functions using time-varying metamaterials," *Appl. Phys. Lett.*, vol. 118, no. 10, Mar. 2021, Art. no. 101901.
[40] V. Pacheco-Peña and N. Engheta, "Effective medium concept in temporal metamaterials," *Nanophotonics*, vol. 9, no. 2, pp. 379–391, Feb. 2020.
[41] V. Pacheco-Peña and N. Engheta, "Anti-reflection temporal coatings," *Optica*, vol. 7, no. 4, pp. 323–331, Mar. 2020.
[42] H. Li and A. Alù, "Temporal switching to extend the bandwidth of thin absorbers," *Optica*, vol. 8, no. 1, p. 24, Jan. 2021.
[43] D. Ramaccia, D. L. Sounas, A. Alù, A. Toscano, and F. Bilotti, "Doppler cloak restores invisibility to objects in relativistic motion," *Phys. Rev. B, Condens. Matter*, vol. 95, no. 7, Feb. 2017, Art. no. 075113.
[44] X. Wan *et al.*, "Multichannel direct transmissions of near-field information," *Light, Sci. Appl.*, vol. 8, no. 1, p. 60, Dec. 2019.
[45] J. Y. Dai *et al.*, "High-efficiency synthesizer for spatial waves based on space-time-coding digital metasurface," *Laser Photon. Rev.*, vol. 14, no. 6, Jun. 2020, Art. no. 1900133.
[46] J. W. Zang, D. Correas-Serrano, J. T. S. Do, X. Liu, A. Alvarez-Melcon, and J. S. Gomez-Diaz, "Nonreciprocal wavefront engineering with time-modulated gradient metasurfaces," *Phys. Rev. Appl.*, vol. 11, no. 5, May 2019, Art. no. 054054.
[47] A. E. Cardin *et al.*, "Surface-wave-assisted nonreciprocity in spatio-temporally modulated metasurfaces," *Nature Commun.*, vol. 11, no. 1, pp. 1–9, Dec. 2020.
[48] S. Taravati and G. V. Eleftheriades, "Full-duplex nonreciprocal beam steering by time-modulated phase-gradient metasurfaces," *Phys. Rev. Appl.*, vol. 14, no. 1, Jul. 2020, Art. no. 014027.
[49] Y. Hadad, J. C. Soric, and A. Alu, "Breaking temporal symmetries for emission and absorption," *Proc. Nat. Acad. Sci. USA*, vol. 113, no. 13, pp. 3471–3475, Mar. 2016.
[50] L. Zhang *et al.*, "Dynamically realizing arbitrary multi-bit programmable phases using a 2-bit time-domain coding metasurface," *IEEE Trans. Antennas Propag.*, vol. 68, no. 4, pp. 2984–2992, Apr. 2020.
[51] J. Y. Dai *et al.*, "Arbitrary manipulations of dual harmonics and their wave behaviors based on space-time-coding digital metasurface," *Appl. Phys. Rev.*, vol. 7, no. 4, Dec. 2020, Art. no. 041408.
[52] J. Y. Dai *et al.*, "Realization of multi-modulation schemes for wireless communication by time-domain digital coding metasurface," *IEEE Trans. Antennas Propag.*, vol. 68, no. 3, pp. 1618–1627, Mar. 2020.
[53] J. A. Hodge, K. V. Mishra, and A. I. Zaghloul, "Intelligent time-varying metasurface transceiver for index modulation in 6G wireless networks," *IEEE Antennas and Wireless Propag. Lett.*, vol. 19, no. 11, pp. 1891–1895, Nov. 2020.
[54] Q. Wu and R. Zhang, "Towards smart and reconfigurable environment: Intelligent reflecting surface aided wireless network," *IEEE Commun. Mag.*, vol. 58, no. 1, pp. 106–112, Jan. 2019.
[55] X. Wang and C. Caloz, "Spread-spectrum selective camouflaging based on time-modulated metasurface," *IEEE Trans. Antennas Propag.*, vol. 69, no. 1, pp. 286–295, Jan. 2021.
[56] J. M. Manley and H. E. Rowe, "Some general properties of nonlinear elements—Part I. General energy relations," *Proc. IRE*, vol. 44, no. 7, pp. 904–913, Jul. 1956.
[57] H. E. Rowe, "Some general properties of nonlinear elements. II. Small signal theory," *Proc. IRE*, vol. 46, no. 5, pp. 850–860, May 1958.
[58] C. He, X. Liang, Z. Li, J. Geng, and R. Jin, "Direction finding by time-modulated array with harmonic characteristic analysis," *IEEE Antennas Wireless Propag. Lett.*, vol. 14, pp. 642–645, 2015.
[59] J. Chen *et al.*, "Direction finding of linear frequency modulation signal with time-modulated array," *IEEE Trans. Antennas Propag.*, vol. 67, no. 4, pp. 2841–2846, Apr. 2019.
[60] J. Chen *et al.*, "Direction finding of linear frequency modulation signal in time modulated array with pulse compression," *IEEE Trans. Antennas Propag.*, vol. 68, no. 1, pp. 509–520, Jan. 2020.
[61] Y. Youn, J. Kim, S. Oh, and S.-H. Yi, "Time-modulated array system controlled with bipolar squared periodic sequence for direction of arrival estimation," *IEEE Wireless Commun. Lett.*, vol. 10, no. 9, pp. 1895–1898, Sep. 2021.
[62] J. Wei Wang *et al.*, "High-precision direction-of-arrival estimations using digital programmable metasurface," *Adv. Intell. Syst.*, vol. 4, no. 4, Apr. 2022, Art. no. 2100164.
[63] A. M. Yao, W. Wu, and D. G. Fang, "Single-sideband time-modulated phased array," *IEEE Trans. Antennas Propag.*, vol. 63, no. 5, pp. 1957–1968, May 2015.
[64] C. Balanis, *Antenna Theory: Analysis and Design*, 4th ed. Hoboken, NJ, USA: Wiley, 2006.
[65] *Infineon BAR65-03W PIN Diode, Datasheet and Models*. [Online]. Available: https://www.infineon.com/cms/en/product/rf/rf-diode/rf-pin-diode/antenna-switch/bar63-03w/
[66] *CST—Computer Simulation Technology*. Accessed: Apr. 12, 2019. [Online]. Available: https://www.cst.com/
[67] H. Yang *et al.*, "A 1-bit 10×10 reconfigurable reflectarray antenna: Design, optimization, and experiment," *IEEE Trans. Antennas Propag.*, vol. 64, no. 6, pp. 2246–2254, Jun. 2016.
[68] Y. Wang, S. Xu, F. Yang, and D. H. Werner, "1 bit dual-linear polarized reconfigurable transmitarray antenna using asymmetric dipole elements with parasitic bypass dipoles," *IEEE Trans. Antennas Propag.*, vol. 69, no. 2, pp. 1188–1192, Feb. 2021.

Xinyu Fang was born in Inner Mongolia, China. He received the B.E. degree in electronic information engineering from the Nanjing University of Science and Technology, Nanjing, China, in 2019, where he is currently pursuing the Ph.D. degree in electronic science and technology.

His current research interests include metasurface, antenna design, and space–time-modulated array.

Mengmeng Li (Senior Member, IEEE) received the B.S. degree (Hons.) in physics from Huaiyin Normal College, Huai'an, China, in 2007, and the Ph.D. degree in electromagnetic field and microwave technology from the Nanjing University of Science and Technology (NJUST), Nanjing, China, in 2014.

From 2012 to 2014, he was a Visiting Student with the Electronics Department, Politecnico di Torino, Turin, Italy, and also with the Antenna and EMC Laboratory (LACE), Istituto Superiore Mario Boella, Turin, where he carried out fast solver for multiscale simulations. Since 2014, he has been with the Department of Communication Engineering, NJUST, where he has been an Assistant Professor, an Associate Professor, and a Professor, since 2020. In 2017, he joined Pennsylvania State University, Pennsylvania, PA, USA, as a Visiting Scholar. His current research interests include fast solver algorithms, computational electromagnetic solvers for circuits, signal integrity analysis, and multiscale simulations.

Dr. Li was a recipient of the Doctoral Dissertation Award of Jiangsu Province in 2016, the Young Scientist Award at the ACES-China Conference in 2019, and five student paper/contest awards at the international conferences with the students. He is an active reviewer for many IEEE journals and conferences. He is an Associate Editor of the *IEEE Antennas and Propagation Magazine*, IEEE Open Journal of Antennas and Propagation (OJAP), and IEEE Access, and a Guest Editor of IEEE OJAP.

Juzheng Han was born in Jiangsu, China, in 1991. She received the B.S. degree from Northeastern University, Shenyang, China, in 2012, and the Ph.D. degree from Southeast University, Nanjing, China, in 2017.

Since 2017, she has been working with the Nanjing University of Science and Technology, Nanjing, and is currently an Associate Professor. Her research interests include microwave device, RF MEMS, and metasurface.

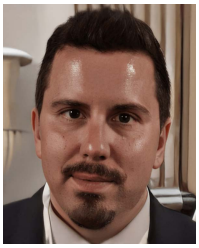

Davide Ramaccia (Senior Member, IEEE) received the B.S. and M.S. degrees (*summa cum laude*) in electronic and ICT engineering and the Ph.D. degree in electronic engineering from Roma Tre University, Rome, Italy, in 2007, 2009, and 2013, respectively.

From 2013 to 2021, he was with the Department of Engineering, Roma Tre University, where he has been with the Department of Industrial, Electronic, and Mechanical Engineering since 2021. He has coauthored more than 100 articles in international journals, conference proceedings, and book chapters, and holds one patent. His main research interests are in the modeling and design of (space-)time-varying metamaterials and metasurfaces, and their applications to microwave components and antennas, and the analysis of anomalous scattering effects in temporal metamaterials.

Dr. Ramaccia was a recipient of a number of awards and recognitions, including the Electromagnetics Academy Young Scientist Award in 2019, seven outstanding reviewer awards by the IEEE TRANSACTIONS ON ANTENNAS AND PROPAGATION from 2013 to 2021, the IET prizes for the best poster on microwave metamaterials in 2013, and IET Award for the best poster on the metamaterial application in antenna field in 2011. He has been serving on the scientific community, by playing roles in the management of scientific societies, in the editorial board of international journals, and in the organization of conferences and courses. He is currently the General Secretary of the Virtual Institute for Artificial Electromagnetic Materials and Metamaterials (METAMORPHOSE VI, the International Metamaterials Society) and has been an Elected Member of the Board of Directors of the same association for three consecutive terms since 2014. In 2022, he is appointed as a member of the IEEE APS Award Committee by the IEEE APS Society. He has been serving as an Associate Editor for the IEEE ACCESS since 2019, a Scientific Moderator for IEEE TechRxiv since 2019, and a Technical Reviewer for the major international journals related to electromagnetic field theory and metamaterials. He was also a Guest Coeditor of three special issues on metamaterials and metasurfaces. Since 2015, he has been serving as a member of the Steering Committee of the International Congress on Advanced Electromagnetic Materials in Microwaves and Optics—Metamaterials Congress. He was the General Chair and a Local Organizer of the 39th and 42nd EUPROMETA Doctoral School on Metamaterials held in Rome, in 2019 and 2021, respectively. He was a Technical Program Coordinator (Track "Electromagnetics and Materials") for the 2016 IEEE Antennas and Propagation Symposium. He is a member of the Technical Program Committee of the International Congress on Laser Science and Photonics Applications—CLEO 2022. He was elected as a Secretary of the Project Management Board of the H2020 CSA project NANOARCHITECTRONICS from 2017 to 2018.

Alessandro Toscano (Senior Member, IEEE) was born in Capua, Italy, in 1964. He received the B.S. and Ph.D. degrees in electronic engineering from the Sapienza University of Rome, Rome, Italy, in 1988 and 1993, respectively.

Since 2011, he has been a Full Professor of Electromagnetic Fields with the Engineering Department, Roma Tre University, Rome. He carries out an intense academic and scientific activity, both nationally and internationally. From April 2013 to January 2018, he was a member of Roma Tre University Academic Senate. From October 2016 to October 2018, he was a member of the National Commission which enables National Scientific Qualifications to Full and Associate Professor in the tender sector 09/F1—electromagnetic fields. Since January 2018, he has been the Vice-Rector for Innovation and Technology Transfer. He has held numerous invited lectures at universities, public and private research institutions, and national and international companies on the subject of artificial electromagnetic materials, metamaterials, and their applications. He actively participated in founding the international association on metamaterials Virtual Institute for Advanced Electromagnetic Materials—METAMORPHOSE, VI. He coordinates and participates in several research projects and contracts funded by national and international public and private research institutions and industries. His scientific research has as ultimate objective the conceiving, designing, and manufacturing of innovative electromagnetic components with a high technological content that show enhanced performance compared to those obtained with traditional technologies and that respond to the need for environment and human health protection. He has authored more than 100 publications in international journals indexed ISI or Scopus; of these on a worldwide scale, three are in the first 0.1 percentile, five in the first 1 percentile, and 25 in the first 5 percentile in terms of the number of quotations and journal quality. His research activities are focused on three fields: metamaterials and unconventional materials, in collaboration with Prof. A. Alù's Group with The University of Texas at Austin, Austin, TX, USA, research and development of electromagnetic cloaking devices and their applications (First Place Winner of the Leonardo Group Innovation Award for the research project titled: Metamaterials and Electromagnetic Invisibility), and the research and manufacturing of innovative antenna systems and miniaturized components (First Place Winner of the Leonardo Group Innovation Award for the research project titled: Use of Metamaterials for Miniaturization of Components—MiniMETRIS).

Prof. Toscano is currently a member of the Board of Director of Radiolabs (a non-for-profit Research Consortium), the Steering Committee of the National Competence Center on Cyber 4.0, and the Scientific Council of CIRIAF (Interuniversity Research Center on Pollution and the Environment). In addition to his commitment in organizing scientific events, he also carries out an intense editorial activity as a member of the review committees of major international journals and conferences in the field of applied electromagnetics.

Filiberto Bilotti (Fellow, IEEE) received the Laurea and Ph.D. degrees in electronic engineering from Roma Tre University, Rome, Italy, in 1998 and 2002, respectively.

He was with the Faculty of Engineering from 2002 to 2012 and the Department of Engineering from 2013 to 2021 with Roma Tre University, where he has been with the Department of Industrial, Electronic, and Mechanical Engineering since 2021, serving as a Full Professor of Electromagnetic Field Theory since 2014, and the Director of the Antennas and Metamaterials Research Laboratory since 2012. His main research contributions are in the analysis and design of microwave antennas and arrays, analytical modeling of artificial electromagnetic materials, metamaterials, and metasurfaces, including their applications at both microwave and optical frequencies. In the last ten years, his main research interests have been focused on the analysis and design of cloaking metasurfaces for antenna systems, on the modeling and applications of (space- and) time-varying metasurfaces, on the topological-based design of antennas supporting structured field, on the modeling, design, implementation, and application of reconfigurable metasurfaces, on the concept of meta-gratings and related applications in optics and at microwaves, and on the modeling and applications of optical metasurfaces. The research activities developed in the last 20 years have resulted in more than 500 articles in international journals, conference proceedings, book chapters, and three patents.

Prof. Bilotti was a recipient of a number of awards and recognitions, including the elevation to the IEEE Fellow Grade for contributions to metamaterials for electromagnetic and antenna applications in 2017, the Outstanding Associate Editor of the IEEE TRANSACTIONS ON ANTENNAS AND PROPAGATION in 2016, the NATO SET Panel Excellence Award in 2016, the Finmeccanica Group Innovation Prize in 2014, the Finmeccanica Corporate Innovation Prize in 2014, the IET Best Poster Paper Award (Metamaterials 2013 and Metamaterials 2011), and the Raj Mittra Travel Grant Senior Researcher Award in 2007. He has been serving the scientific community, by playing leading roles in the management of scientific societies, in the editorial board of international journals, and in the organization of conferences and courses. In particular, he was a Founding Member of

the Virtual Institute for Artificial Electromagnetic Materials and Metamaterials—METAMORPHOSE VI, in 2007. He was elected as a member of the Board of Directors of the same society for two terms from 2007 to 2013 and as the President for two terms from 2013 to 2019. He currently serves as the Vice-President of METAMORPHOSE VI and has been the Executive Director since 2019. He served as an Associate Editor for the IEEE TRANSACTIONS ON ANTENNAS AND PROPAGATION from 2013 to 2017 and the *Metamaterials* from 2007 to 2013 and as a member of the Editorial Board of the *International Journal on RF and Microwave Computer-Aided Engineering* from 2009 to 2015, *Nature Scientific Reports* from 2013 to 2016, and *EPJ Applied Metamaterials* since 2013. He was also the Guest Editor of five special issues in international journals. In 2007, he hosted the inaugural edition of the International Congress on Advanced Electromagnetic Materials in Microwaves and Optics—Metamaterials Congress, served as the Chair of the Steering Committee of the same conference for eight editions from 2008 to 2014 and 2019, and was elected as the General Chair of the Metamaterials Congress for the period from 2015 to 2018. He was also the General Chair of the Second International Workshop on Metamaterials-by-Design Theory, Methods, and Applications to Communications and Sensing in 2016 and has been serving as the Chair or a member of the technical program, steering, and organizing committee of the main national and international conferences in the field of applied electromagnetics.

Dazhi Ding (Senior Member, IEEE) received the B.Sc. and Ph.D. degrees in electromagnetic field and microwave technique from the Nanjing University of Science and Technology (NJUST), Nanjing, China, in 2002 and 2007, respectively.

In 2005, he joined the Center of Wireless Communication, City University of Hong Kong, Hong Kong, as a Research Assistant. He joined the Department of Electrical Engineering, NJUST, where he became a Lecturer in 2007, was promoted to Full Professor in 2014, and was appointed as the Head of the Department of Communication Engineering, in September 2014. He has authored or coauthored over 30 technical articles and more than 80 articles. His current research interests include computational electromagnetics and electromagnetic scattering and radiation.

Dr. Ding was a recipient of the National Excellent Youth Fund by the National Science Foundation of China (NSFC) in 2020.

Open Access funding provided by 'Università degli Studi Roma Tre' within the CRUI-CARE Agreement